Article | Open Access

Energy Materials

Zhai et al. Energy Mater. 2026, 6, 600046 DOI:10.20517/energymater.2026.11

A high-performance quasi-solid-state supercapacitor diode for flexible logic gate

Dongmei Zhai#, Zefeng Yan#, Keyi Dong, Weiyang Tang, Quanhu Sun, Xiao Li, Jiaxin Yang, Tian Lv, Tao Chen*

Keywords:
Supercapacitor, diode, logic gate, quasi-solid-state, flexible

Citation: Zhai, D.; Yan, Z.; Dong, K.; Tang, W.; Sun, Q.; Li, X.; Yang, J.; Lv, T.; Chen, T. A high-performance quasi-solid-state supercapacitor diode for flexible logic gate. *Energy Mater.* **2026**, *6*, 600046. https://dx.doi.org/10.20517/energymater.2026.11

Received: 25 Jan 2026
First Decision: 28 Feb 2026
Revised: 26 Mar 2026
Accepted: 14 Apr 2026
Published: 6 May 2026

Academic Editor:
Jung Ho Kim
Copy Editor:
Pei-Yun Wang
Production Editor:
Pei-Yun Wang

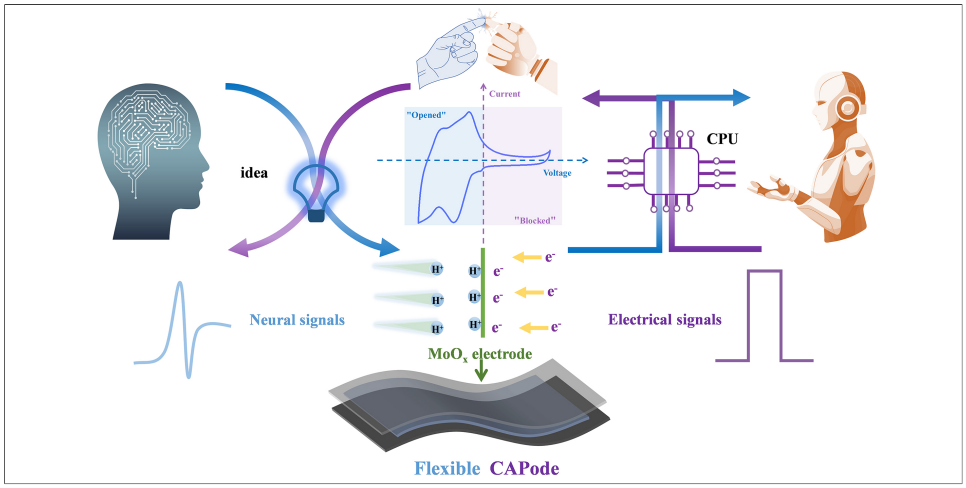

Abstract

A supercapacitor diode (CAPode), which combines both functions of energy storage and the current rectification, shows strong potential for a wide range of applications. However, it remains a big challenge to achieve flexible CAPodes with high performance because of limitations in electrode and electrolyte materials. In this study, we construct a high-performance flexible CAPode by synergistical optimization of electrodes and polymer electrolyte. The ion–sieving effects of oxygen–deficient intercalated transition metal oxide (MoO_x) are revealed by experimental results and theoretical calculation. The resultant quasi-solid-state CAPode not only shows high specific capacitance and rectification ratio, but also exhibits excellent mechanical flexibility. The CAPodes-based "AND" and "OR" logic gates with good processing ability are also built and investigated.

INTRODUCTION

With the rapid development of flexible portable electronic devices in fields such as intelligent sensing, human–computer interaction and brain–computer interfaces, there is an urgent need to develop highly integrated multifunctional devices, to

Shanghai Key Lab of Chemical Assessment and Sustainability, School of Chemical Science and Engineering, Tongji University, Shanghai 200092, China.
#Equally contributed to this work.

***Correspondence to:** Prof. Tao Chen, Shanghai Key Lab of Chemical Assessment and Sustainability, School of Chemical Science and Engineering, Tongji University, Shanghai 200092, China. E-mail: tchen@tongji.edu.cn

overcome structural and material mismatch among them. In most electronics, energy storage device and diode–based logic circuit are the essential components, but they are often independent with each other. As one of the most important energy-storage devices, a supercapacitor (also known as electrochemical capacitor) stores electrical energy through ions absorption in/on electrodes or through Faraday redox reactions of active materials. Supercapacitors possess ultrahigh power density and long cycle life, making them a promising energy-supply devices for a wide range of electronics[1-4]. Many efforts have been made to provide the supercapacitors with multi–functions by functionalizing of active materials and electrolytes[5-8]. Semiconductor diodes that allow the current to pass through in a certain direction are indispensable building blocks for current rectification, switching, transistor, logic circuits, and so on. Therefore, an energy-storage device with diode-like characteristics that can serve as a unit for constructing logic circuits would be highly valuable for the integration and miniaturization of electronic devices.

In 2019, Zhang *et al.* firstly proposed a new type of supercapacitor diode (CAPode) with both unidirectional conduction characteristic of semiconductor diode and capability of energy storage, by engineering the pore sizes of microporous and mesoporous carbon materials as the positive and negative electrodes, respectively[9]. During charging, only anions smaller than the pore size of the microporous carbon can be absorbed into the internal surface of microporous carbon, while cations with larger sizes were blocked. As a result, the CAPode can only be charged in one direction of polarization (so–called open or chargeable, corresponding to the forward bias direction of a diode). On the contrary, little electric energy can be stored as the CAPode is polarized in reverse (also called blocking or non–chargeable direction), corresponding to the reverse bias direction of a diode. The unidirectional chargeable characteristic of CAPode is very similar with the feature of semiconductor diode. Accordingly, the CAPode, which exhibits capacitive behavior in the positive potential range but no capacitive response in the negative potential region, is defined as p–CAPode. In contrast, the n–CAPode has a high current in the negative potential range and will be closed in the positive potential range without capacitive response. Apart from the strategy of engineering the porous size of electrode materials[9,10], polyionic liquid electrolytes were also designed for CAPodes, in which the small movable ions can diffuse into and absorb inside electrode materials, instead of large-size polymers[11]. In addition, CAPodes based on the ion–selective surface redox reaction effect of electrode was first reported by Yan and colleagues[12], while other redox pseudocapacitive materials (e.g., Ni foam[13], $Ni_3Bi_2S_2$[14], $FeCoCrMnNiP_x$[15], layered double hydroxide[16]) were also developed to construct CAPodes. Intercalation/deintercalation of ions in pseudocapacitive materials (e.g., molybdenum oxide[17], orthorhombic niobium pentoxide[18], hexagonal tungstentrioxide[19-21] and carbon-modified anatase titania[22]) have also been demonstrated. Due to the crystal nature and negatively charged properties of the interlayer channels of these metal oxides, the 3D ion transport channels allow intercalation/deintercalation of small cations (e.g., H^+, Li^+), while large-size anions (e.g., ClO_4^-, PF_6^-) were excluded. It should be noted that the reported CAPodes were mostly constructed with liquid electrolytes[9-23], which has the risk of leakage during fabrication and/or usage processes, resulting in performance decay or loss of their functions. To fully take advantage of both functions of current rectification and energy storage, it is urgent to develop flexible CAPodes with high performance for practical applications in portable electronics [Figure 1A].

To address this issue, we demonstrate a flexible CAPode with high electrochemical performance and excellent rectification behavior by assembling an activated carbon positive electrode and a MoO_x negative electrode with a quasi-solid-state polyvinyl alcohol (PVA)/H_3PO_4 polymer electrolyte in between. The synergistic effects of electrode structure and ions size provide the designed device with both features of supercapacitor and diode. As desired, the developed quasi-solid-state CAPode not only exhibits a high specific capacitance of 139.32 F g^{-1}, but also possesses a high rectification ratio I (RR_1) of 14.62 and

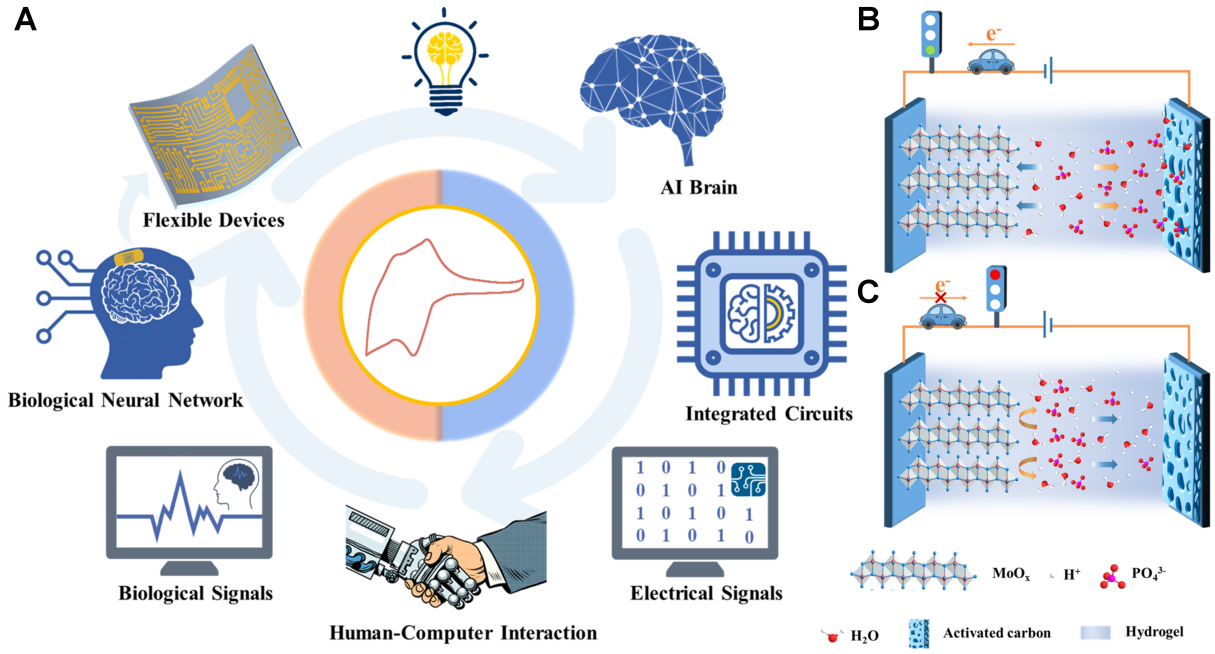

Figure 1. (A) Schematic shows the potential applications of CAPode; (B and C) Schematics show unidirectional charge storage of CAPode: under forward (B) and reverse biases (C).

rectification ratio II (RR_{II}) of 96.18%. Meanwhile, the electrochemical performance and rectification capability of the constructed CAPode changed very slightly under various bending angles and even after 3,000 folding cycles, indicating excellent flexible stability and cyclic reliability. Benefiting from the high rectification performance and energy storage property of the developed CAPode, a quasi-solid-state well–operated ionic logic circuit (AND, OR) is constructed. The flexible quasi-solid-state CAPode integrated with both functions of diode and energy storage has potential to be used in integrated circuits, smart grids, and brain–computer interfaces.

EXPERIMENTAL

Preparation of MoO_x/CNTs and AC/CNTs composite electrodes

MoO_x powder, carbon black (Super P, SZKejing, Shenzhen), and polyvinylidene fluoride (PVDF, SZKejing, Shenzhen) binder were dispersed in a N-methyl-2-pyrrolidone (NMP, AR, Aladdin, Shanghai) with a mass ratio of 8:1:1. Then, the mixture was stirred under a speed of 200 rpm at room temperature for 8 h to form a homogeneous slurry. The slurry was blade–coated on carbon nanotube (CNT) film and dried at 60 °C for 12 h, achieved MoO_x/CNTs film electrode. The thickness of the doctor blades was 100 μm, and the mass loading of MoO_x in MoO_x/CNTs film was 1.5 mg cm^{-2}. As for active carbon (AC)/CNTs composite electrode, AC powder (XFNANO, Jiangsu), carbon black, and PVDF binder were dispersed in a NMP with a mass ratio of 8:1:1. Then, the mixture was stirred under a speed of 200 rpm at room temperature for 8 h to form a homogeneous slurry. The slurry was blade–coated on CNT film and dried at 60 °C for 12 h, formed the AC/CNTs composite electrode. The thickness of the doctor blades was 300 μm, and the mass loading of AC in AC/CNTs film was 4 mg cm^{-2}.

Assembly of CAPode

PVA/H_3PO_4 electrolyte (60 μL) was drop–coated on a piece of positive AC/CNTs electrode. Then, the above electrode was placed in a vacuum oven to make more polymer electrolyte infiltrating into electrode. The CAPode was assembled by pressing one AC/CNTs electrode coated with PVA/H_3PO_4 electrolyte and another negative MoO_x/CNTs electrode together.

Characterization

Scanning electron microscopy (SEM) images were obtained by high-resolution field emission scanning electron microscopy (FESEM, Hitachi S–4800, Japan) with an accelerating voltage of 5 kV. Transmission electron microscopy (TEM) images and selected area electron diffraction (SAED) patterns were taken out by high-resolution transmission electron microscopy (HRTEM, JEOL–2010, Japan). The X-ray diffraction patterns were characterized by X-ray diffraction spectroscopy (XRD, D8 Advance, Bruker, Germany) with Cu–kα radiation (V = 30 kV, I = 25 mA). X-ray photoelectron spectroscopy (XPS) spectra were collected by using Shimadzu Kratos, AXIS Ultra DL (Japan), and the binding energy data were corrected to C 1s = 284.6 eV. Renishaw Raman spectrometer (Britain) equipped with a 514 nm laser is used to characterize the structure of electrode materials.

Electrochemical measurements

The electrochemical performance was measured by an electrochemical working station (CHI 760 E, Shanghai Chenhua). The current-voltage (I-V) characteristics of the devices were measured on a source meter (2400, Keithley, America). Unless specifically mentioned, all the electrochemical performances is calculated based on active materials (i.e., MoO_x, AC), and the related formulas are shown in Supplementary Materials.

RESULTS AND DISCUSSION

The working mechanism of quasi-solid-state CAPode based on MoO_x, AC electrode and PVA/H_3PO_4 electrolyte can be concluded as following. The compact crystal structure of MoO_x only allows intercalating of small cations, the ion transport channels inside MoO_x surrounded by the negatively charged oxygen terminals prefer intercalation/deintercalation of positive ions. As the CAPode is charged with MoO_x served as working and negative electrode (forward bias), the small ions of H^+ in the electrolyte can enter the MoO_x active sites, and the anions of PO_4^{3-} were adsorbed in the pores of AC electrode [Figure 1B]. As a result, the whole device that can be charged normally exhibits the characteristic of supercapacitor. By contrast, under reverse bias, MoO_x serve as the working and positive electrode of the CAPode. Because of electrostatic repulsion, the large PO_4^{3-} anions can only be adsorbed on the outer surface of MoO_x, and therefore cannot occupy the active sites within the material [Figure 1C], showing limited energy storage capacity.

Fabrication and characterization of flexible electrodes

MoO_x nanobelts containing abundant oxygen vacancies were prepared by a one–step hydrothermal method (see the experimental section for details). The crystal morphology of MoO_x nanobelts was investigated by HRTEM [Figure 2A and Supplementary Figure 1], from which mutually perpendicular lattice stripes of MoO_x nanobelts can be observed. The lattice spaces of 0.18 and 0.2 nm [Figure 2A] were corresponded to the (002) and (100) crystal planes at 90° angle in the SAED diagrams [Figure 2B], respectively. Many discontinuities or distortions in the MoO_x lattice stripes can be observed in the HRTEM images, which indicated the presence of oxygen vacancies in the MoO_x nanobelts. The SEM image [Figure 2C] and energy-dispersive X-ray spectroscopy (EDS) elemental mapping [Figure 2D and E] showed that the elements of molybdenum and oxygen were uniformly distributed in the MoO_x nanobelts. From Supplementary Figure 2, it can be seen that the as–synthesized MoO_x had a nanobelt structure with a width of about 300 nm and a length of 10 μm. The XRD pattern of MoO_x [Supplementary Figure 3] showed obvious diffraction peaks at (020), (040) and (060) crystal planes, which well matched with the reference card of MoO_3 (PDF#05–0508), confirming its monoclinic phase derived from an orthorhombic phase with Panm space[24,25].

The Raman spectrum of MoO_x in Supplementary Figure 4 appeared typical fingerprint vibrational modes at 291, 666, 819 and 996 cm^{-1}. More specifically, the Raman peak at 291 cm^{-1} represented the swing mode of the double bond O=Mo=O, whereas the Raman peaks at 666, 819, and 996 cm^{-1} responded to the stretching

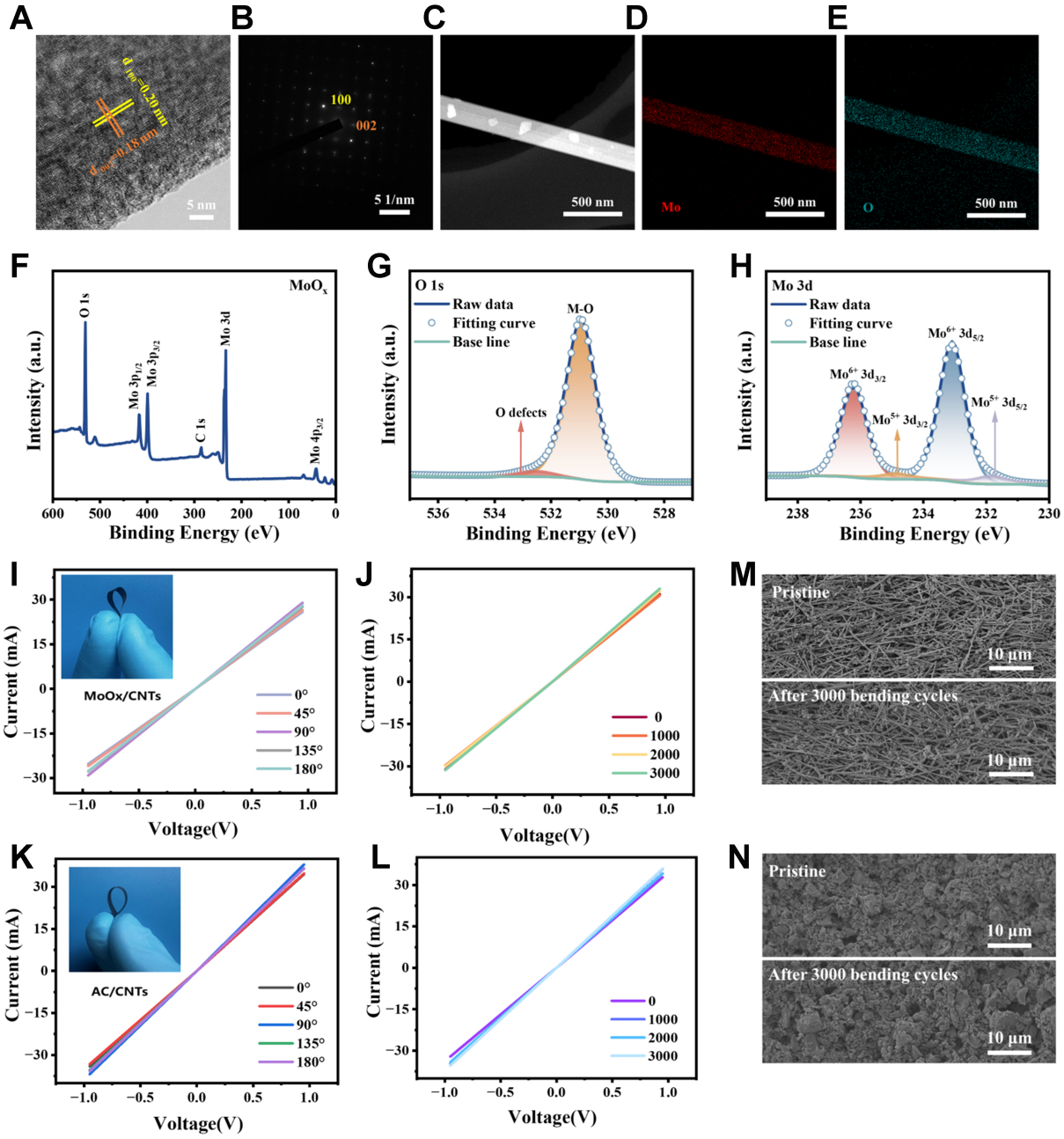

Figure 2. Characterizations of the synthesized MoO_x nanobelts, MoO_x/CNTs and AC/CNTs electrode. (A and B) TEM image (A) and the corresponding SAED pattern (B) of MoO_x nanobelt; (C-E) SEM image (C) and elemental mapping images (D-E) of MoO_x nanobelt; (F-H) XPS spectra of MoO_x nanobelts; (I and J) I-V curves of MoO_x/CNTs electrode under different bending angles (I) and being bent to 135° for different cycles (J). Inset in (I) is the photograph by a digital camera of a bending MoO_x/CNTs electrode; (K and L) I-V curves of AC/CNTs electrode under different bending angles (K) and being bent to 135° for different cycles (L). Inset in (K) is digital photograph by a digital camera of AC/CNTs electrode; (M and N) SEM images of MoO_x/CNTs (M) and AC/CNTs (N) electrode before and after bent to 135° for 3,000 cycles. CNTs: Carbon nanotubes; AC: active carbon; TEM: transmission electron microscopy; SAED: selected area electron diffraction; SEM: scanning electron microscopy; XPS: X-ray photoelectron spectroscopy; I-V: current-voltage.

modes of the triple–coordinated oxygen (Mo–O_s), double–coordinated oxygen (Mo–O_a), and terminal oxygen (Mo=O_t), respectively. Figure 2F showed the XPS full spectrum of MoO_x, which appeared typical peaks of Mo 3p, Mo 3d, and O 1s. The XPS spectrum of O 1s in MoO_x [Figure 2G] showed the presence of oxygen defects in addition to lattice oxygen. The oxygen vacancies in MoO_x nanobelts can expand the Van der Waals gap and regulate the electronic structure of Mo atoms, which will result in enhancement of the charge

storage kinetics and the capacity of MoO_x[26,27]. The fine spectra of MoO_x [Figure 2H] had a twin peak of Mo $3d_{3/2}$ at 236.23 eV and Mo $3d_{5/2}$ at 233.07 eV. The XPS result showed that MoO_x was mainly composed of Mo^{6+} ions (90.11%) and a small percentage of Mo^{5+} ions (9.89%).

CNT films were used as current collectors to load active materials of MoO_x and AC, and PVDF used as binders. From Figure 2I to L, all the I-V curves of both MoO_x/CNTs electrode and AC/CNTs electrode well remained as they were bent to different angles and after different bending cycles, indicating no obvious changes of their electrical conductivities. The SEM results [Figure 2M and N, Supplementary Figures 5 and 6] showed that the conductive networks composed of MoO_x nanobelts and AC almost unchanged after 1,000-3,000 bending cycles. The excellent structural and electric stabilities of electrodes play an important role in the following demonstrated flexible CAPode devices.

The adsorption energies of H^+ and PO_4^{3-} ions at various active sites in MoO_x were calculated using density functional theory (DFT), providing a theoretical evaluation of the ion sieving capacity of MoO_x. Supplementary Figure 7 present the adsorption energies of H^+ and PO_4^{3-} ions on two types of oxygen sites. The adsorption energies for H^+ ions on O_t and O_a are about -0.66 and -0.88 eV, respectively, which indicates that H^+ ions can readily interact with both terminal and asymmetric oxygen sites, facilitating their intercalation into MoO_x. In contrast, the larger-size PO_4^{3-} ions and their electrostatic repulsion with negatively charged oxygen atoms result in much higher adsorption energies of 6.99 eV on O_t and 8.52 eV on O_a. As a result, the small ions of H^+ in the electrolyte can easily intercalate the MoO_x active sites, making the CAPode chargeable under forward bias.

Electrochemical performance of CAPodes

As shown in Figure 3A, the CAPode was assembled by directly pressing one electrode of MoO_x/CNT and another electrode of AC/CNTs together with the polymer electrolyte in between. The cross-sectional SEM image of the whole device [Supplementary Figure 8] showed that the CAPode had a typical sandwiched structure, and the thickness of MoO_x and AC was about 12 and 50 μm, respectively. The thickness of PVA/H_3PO_4 was about 50 μm. Figure 3B and C showed cyclic voltammetry (CV) curves of the CAPode, which exhibited a typical asymmetric shape. From the CV curves, it can be seen that the CAPode prossessed a unidirectional charging characteristic with a threshold voltage of about 0 V. This unidirectional charging behavior can be attributed to the selective intercalation/deintercalation of ions in/out MoO_x. In the negative voltage range from -0.95 to 0 V, the small cations of H^+ can intercalate into and de-intercalate from interlamination of MoO_x, which was corresponding with pseudocapacitive redox peaks in CV curves. In contrast, there was negligible response current in the voltage range from 0 to +0.95 V, because only limited large-size PO_4^{3-} anions were absorbed on the external surface of MoO_x electrode. The large difference of response current between the positive and negative voltage regions revealed the excellent ion–sieving ability of the MoO_x electrode. When the scan rate increased from 10 to 60 mV s^{-1}, the shape of CV curves remained almost the same, the peak current increased linearly with the threshold voltage stabilized at about 0 V, suggesting the rapid intercalation and deintercalation process of H^+ ions. The rectification capability of CAPode is evaluated by RR_I and RR_{II}. RR_I is defined as the ratio of the redox peak currents in negative and positive voltage ranges, and RR_{II} is defined as the ratio of the capacitances in negative and positive voltage ranges[11]. Benefiting from the charge storage capability of MoO_x under negative bias, the RR_I of the developed CAPode reached a maximum value of 14.62 at a scan rate of 10 mV s^{-1}, and remained as high as 10.82 even at a higher scan rate of 60 mV s^{-1}, indicating excellent rectification performance [Figure 3C].

As shown in Figure 3D and E, the galvanostatic charge–discharge (GCD) curves of the CAPode under different current densities had a shape of quasi-triangle, and also exhibited a unidirectional charging behavior. Almost all of the capacity of the CAPode was contributed by the potential range from -0.95 to 0 V,

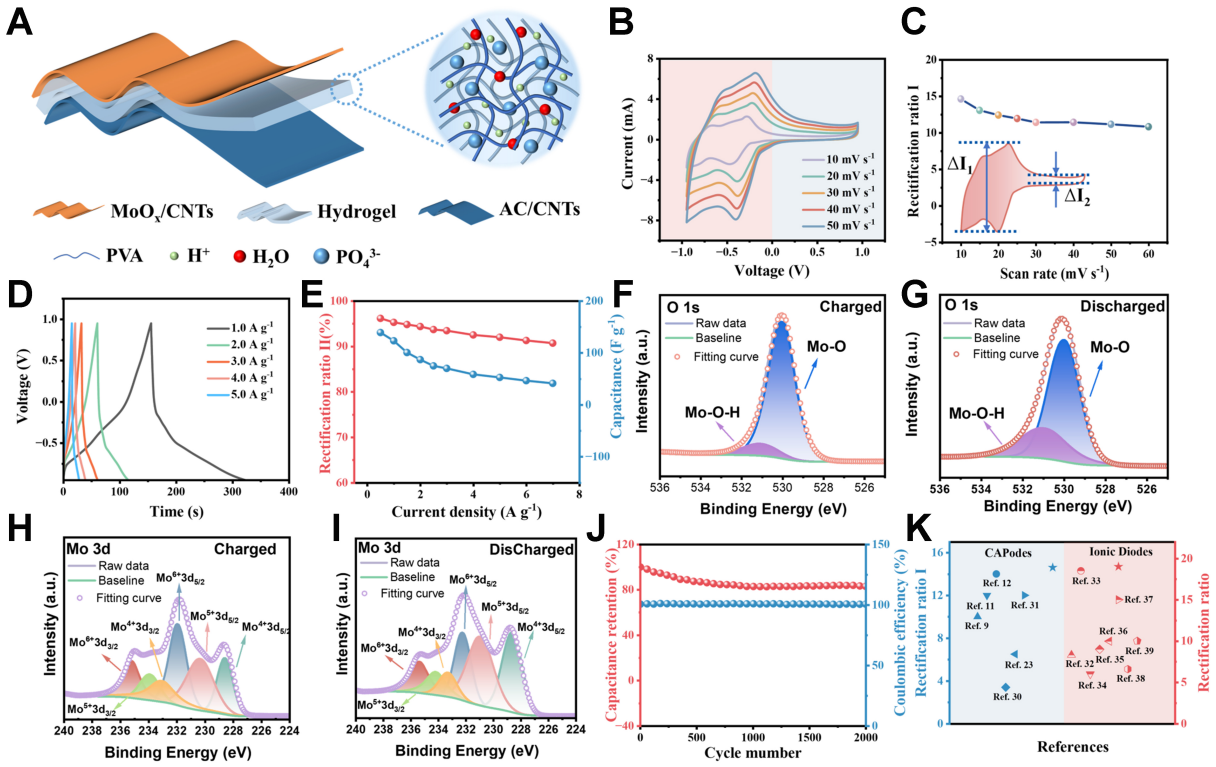

Figure 3. Electrochemical and rectification performances of polymer electrolyte–based CAPode. (A) Schematic structure of flexible CAPode; (B) CV curves at different scan rates; (C) RR_I at different scan rates; (D) GCD curves at different charge/discharge current densities; (E) RR_{II} and specific capacitance at different current densities; (F-I) O 1s (F and G) and Mo 3d (H and I) XPS spectra of MoO_x electrode at fully charged and discharged states; (J) Cycling stability of CAPode at 2 A g^{-1}; (K) Performance comparison of CAPode with other reported CAPodes and ionic diodes. CV: Cyclic voltammetry; RR_I: rectification ratio I; GCD: galvanostatic charge–discharge; RR_{II}: rectification ratio II; XPS: X-ray photoelectron spectroscopy; AC: active carbon; CNTs: carbon nanotubes; PVA: polyvinyl alcohol.

which was highly consistent with the results of the CV tests. The specific capacitance and RR_{II} of the MoO_x–based quasi-solid-state CAPode were further calculated according to the GCD curves. As shown in Figure 3E, the specific capacitance of the MoO_x–based CAPode reached 139.32 F g^{-1} at the current density of 0.5 A g^{-1}, and the RR_{II} of the CAPode was as high as 96.18%. Even the charge/discharge current density further increased to 7 A g^{-1}, the MoO_x–based quasi-solid-state CAPode also exhibited a high specific capacitance of 41.34 F g^{-1} and a RR_{II} of 90.73%, indicating its excellent rate capability.

To further reveal the charge storage mechanism and valence bonds' changes of MoO_x electrode during process of charging/discharging, *in-situ* XPS of MoO_x was conducted, with MoO_x as working electrode, AC as counter electrode, Ag/AgCl as reference electrode, and 0.2 M H_3PO_4 solution as electrolyte, respectively. From XPS spectra of O 1s and Mo 3d in MoO_x electrode at different states [Figure 3F-I], it can be seen that Mo^{6+} and Mo–O species decreased at discharged state, while the Mo^{5+}, Mo^{4+} and Mo–O–H species increased obviously. It can be concluded that the redox centers were the molybdenum atoms in MoO_x electrode, and Mo–O bonds also played an important role to allow H^+ intercalation.

As shown in Figure 3J, the MoO_x–based quasi-solid-state CAPode can maintain 83% of the original capacity and almost 100% of the original coulombic efficiency after 2,000 charge/discharge cycles at a high current density of 2.0 A g^{-1}, which indicated the CAPode with excellent cycling performance

[Supplementary Figures 9 and 10]. Compared with other cations, we used PVA/H_3PO_4 as the gel electrolyte, due to H^+ ions can provide relatively fast ion transport kinetics and high energy storage ability. For comparison, several commonly used gel electrolytes (PVA/LiCl, PVA/KOH, PVA/H_2SO_4, and PVA/$HClO_4$) were also investigated to validate their feasibility for CAPodes. As Supplementary Figures 11 and 12 showed, the response currents of CAPodes based on both electrolytes of PVA/LiCl and PVA/KOH in the potential range from -0.95 to 0 V were much lower than that of CAPode based on PVA/H_3PO_4 electrolyte, resulting in lower rectifications (RR_{II} = 79.52% and 84.86%), respectively, due to the sizes of Li^+ and K^+ larger than H^+. The CAPode based on electrolytes of PVA/H_2SO_4 and PVA/$HClO_4$ delivered RR_{II} ranging from 96.12% to 95.26% [Supplementary Figures 13 and 14], but their cycling stabilities [Supplementary Figure 15] were rather low, because the strong acidity of H_2SO_4 and $HClO_4$ will inevitably corrode the MoO_x electrode material. Although the polymer chains may hinder ions movement of polymeric electrolytes[28,29], our CAPodes achieved a well balance between energy storage efficiency and rectification performance through tuning the ionizable components of the electrolytes. For comparison, the constructed CAPode not only possessed high energy storage capacity and stability, but also exhibited comparable rectification capability with reported CAPodes and ion diodes [Figure 3K][9,11,12,23,30-39].

Flexibility of the CAPode

Mechanical flexibility is essential to meet the demands of flexible and wearable electronics[40]. To evaluate the flexible stability of the developed CAPodes, we investigated their rectification ratio and capacitance retentions as the devices under different bending angles and bending cycles. As Figure 4A showed, there were no obvious structural delamination or damage as the prepared device was bent under different angles. It can be seen that both CV [Figure 4B] and GCD [Figure 4C] curves of the CAPode almost overlapped as the device was bent from 0° to 180°. From the electrochemical impedance spectroscopies (EIS, Figure 4D), the series resistance and ionic diffusion ability of the CAPode almost unchanged under different bending angles, which was the reason why the device can well maintain its electrochemical performance under bending states. Even after 3,000 repeated bending cycles from 0° to 180°, all the CV, GCD and EIS curves [Figure 4E-G] still maintained as its original states, which indicated the CAPode with excellent flexible stability.

Rectification performance of the CAPodes

Figure 5A and B schematically showed the simplified equivalent circuits of the CAPode under forward bias and reverse bias, similar to the unidirectional conduction characteristics of semiconductor diodes. A series of EISs under biases from -0.95 to +0.95 V were measured to analyze the rectification performance of the CAPode. From Figure 5C, the impedance in low–frequency region of the Nyquist plot obviously decreased as the bias gradually decreased from 0 to -0.95 V, which revealed the efficient acceleration of ion migration in this process[41,42]. Correspondingly, the phase angle of the Bode phase diagram in the low–frequency region became smaller and smaller with the bias decreasing from 0 to -0.95 V [Figure 5D]. In contrast, both impedance and phase angle slightly increased as the bias increased from 0 to +0.95 V, which revealed that there were few ions contributed to energy storage process because of their large size. The results were well corresponding to the electrochemical behaviors discussed above, which further confirmed the working mechanism of the developed CAPodes.

To evaluate the feasibility of MoO_x–based CAPode for electronic circuits and logic gates, the current rectification capability was investigated by the standard chronoamperometry (CA). Before CA test, the initial open-circuit voltage of CAPode was set at 0 V for a period of time to eliminate the disorderliness of ions until the value of current was stable. As Figure 5E showed, the instantaneous current was as high as 20.22 mA at -0.95 V, while the instantaneous current was as low as 1.86 mA at +0.95 V. After removing of the loading bias voltage, the current response under +0.95 decreased faster than under -0.95 V, due to its mechanism of ions surface adsorption rather the mechanism of intercalation/deintercalation. As a result, a

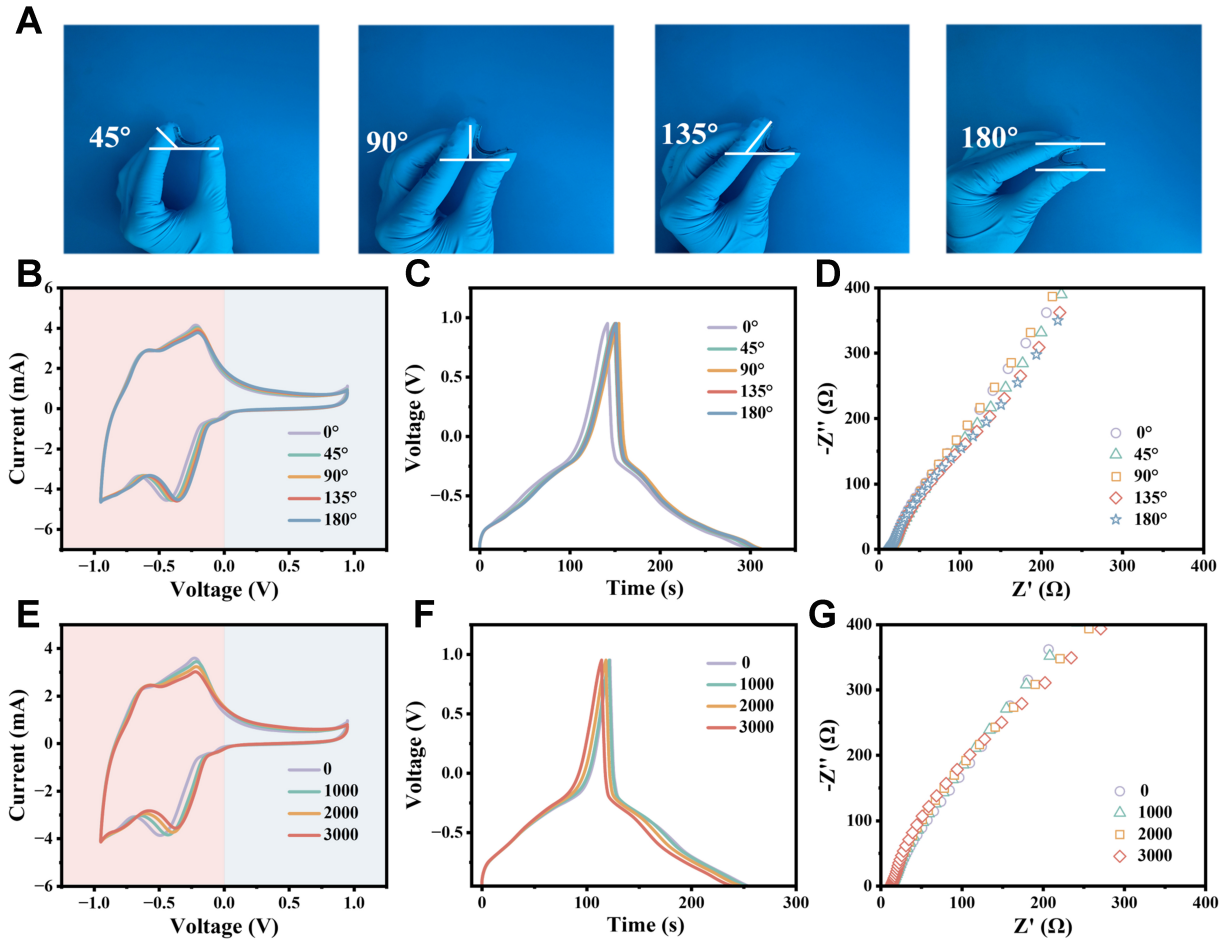

Figure 4. The mechanical flexibility and stability of CAPode based on PVA/H_3PO_4 hydrogel electrolyte. (A) Photographs by a digital camera of flexible CAPode under different bending angles; (B-D) CV curves (B) at a scan rate of 20 mV s^{-1}, GCD curves at a current density of 1 A g^{-1} (C), and Nyquist plots (D) of one CAPode under different bending angles; (E-G) CV curves (E) at a scan rate of 20 mV s^{-1}, GCD curves (F) at a current density of 1 A g^{-1}, and Nyquist plots curves (G) of one N–CAPode being bent to 180 for different cycles. PVA: Polyvinyl alcohol; CV: cyclic voltammetry; GCD: galvanostatic charge–discharge.

rectification ratio of the CAPode between the response currents under negative and positive bias voltages reached a maximum value of 33.6 at 2.2 s and gradually decayed and stabilized at 15.7 after 600 s [Figure 5F], which was obviously different from that of semiconductor diodes (constant rectification ratio after applies bias voltage). Figure 5G showed the current-time (I-t) curves of the CAPode with alternating voltages of -0.95 and +0.95 V applied for 1 s once a time for a few cycles. It can be seen that the final current at -0.95 V was about four times of that at +0.95 V. Both currents will increase with the applied pulse time increasing, but the final current at -0.95 V was always higher than that at +0.95 V [Supplementary Figure 16], due to the intrinsic feature of the CAPode. From I-V curves shown in Figure 5H, the CAPode was on with a charging current of -22.8 mA under -0.95 V, while it was off with a charging current of 1.9 mA under +0.95 V. Distinct "ON" and "OFF" states of the CAPode can also be realized under low forward and reverse bias voltages (e.g., ±0.6 and ±0.3 V, Supplementary Figure 17), suggesting its excellent unidirectional charging capability.

Performance of CAPode in logic gates

The rectification characteristic of the CAPode endows it to be used for transmitting, regulating, and establishing signaling patterns of ions and/or biomolecules[43]. By using two identical CAPodes, logic gates of "AND" and "OR" were constructed and investigated. Figure 6A and B showed the equivalent circuit diagrams of an "AND" logic gate and its corresponding truth table, respectively. In case of the "AND" logic

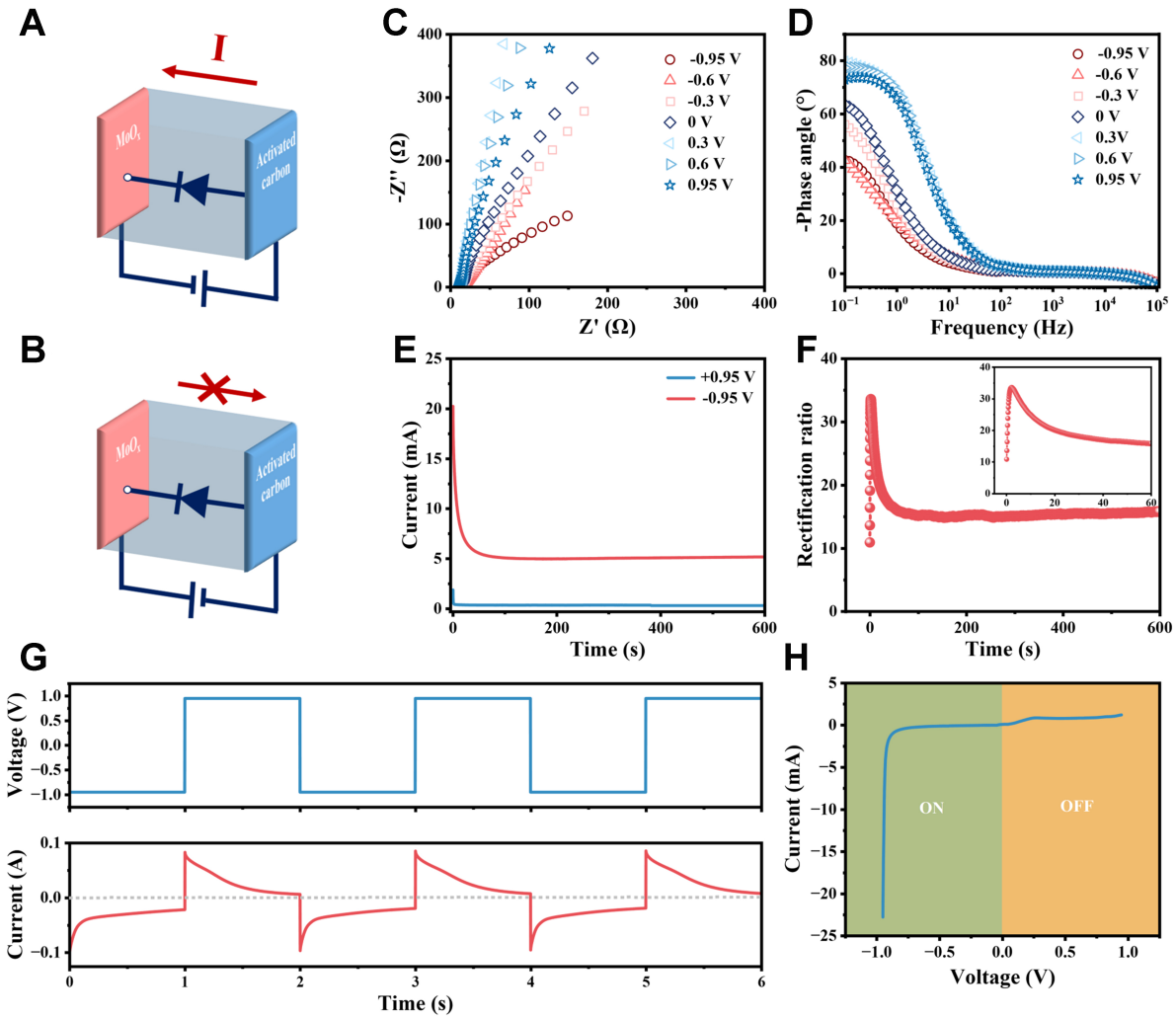

Figure 5. Rectification characteristics of a single CAPode. (A and B) Equivalent circuit diagrams of forward conduction (A) and reverse cutoff (B); (C and D) Nyquist plots (C) and Bode phase plots (D) of CAPode under different biases; (E and F) CA curves of CAPode under the bias voltages of ± 0.95 V (E) and the calculated rectification ratio to the bias application time (F); (G) CA curves of CAPode under alternating voltages of ± 0.95 V, applied for 1s; (H) I-V curve of CAPode. CA: Chronoamperometry; I-V: current-voltage.

gate [Figure 6C], two CAPodes with the same direction were applied a negative bias voltage (-0.95V, denoted as "1"), the entire circuit conducted and output a high current (denoted by "on"). As a positive voltage (+0.95 V, denoted as "0") was applied on two CAPodes, the entire circuit was off, almost without current passing through (denoted by "off"). With one CAPode applied a positive voltage and another CAPode applied a negative voltage, the circuit can also achieve a state of "off", but needing long time. Figure 6D and E showed the equivalent circuit diagram of an "OR" logic gate and its corresponding truth table. For the "OR" logic gate, as a negative bias voltage of -0.95 V was applied to either CAPode A or CAPode B, the circuit was conductive, but the output current was lower than that of both CAPodes applied with a bias voltage of -0.95 V [Figure 6F]. As a positive bias voltage of +0.95 V was applied on both CAPode A and CAPode B at the same time, almost no current can pass through the circuit.

To validate the feasibility of the CAPodes for practical applications, logic gates were constructed to turn on/off a light emitting diode (LED) bulb, with the CAPodes as the power supply at the same time. To meet the voltage requirement of the used LED, two identical CAPode connected in series that had a widen voltage of 1.9 V [Figure 6G and Supplementary Figure 18] were used as one unit of ionic diode to build the logic

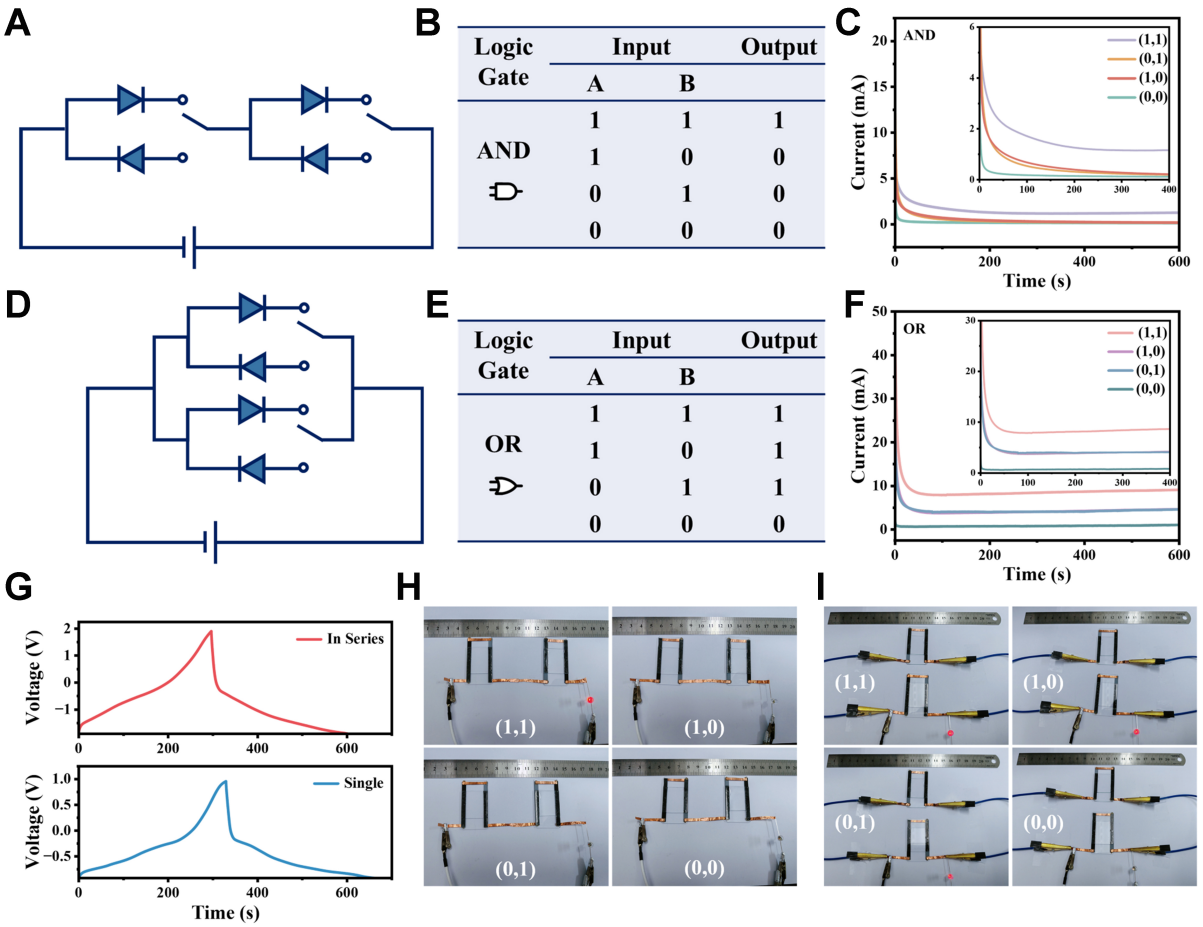

Figure 6. "AND" and "OR" logic gates based on CAPodes. (A-C) Schematic diagram (A), corresponding truth table (B), and output signals of an "AND" logic gate circuit (C); (D-F) Schematic diagram (D), corresponding truth table (E), and output signals of an "OR" logic gate circuit (F); (G) GCD curves of one single and two CAPodes connected in series; (H and I) Photographs by a digital camera of an "AND" gate (H) and an "OR" gate to switch an LED (I). GCD: Galvanostatic charge–discharge; LED: light emitting diode.

gates. CA curves of the logic gates ("AND" and "OR") by alternately applying -1.9 V and +1.9 V under different inputs of [(0, 0), (1, 1), (0, 1) and (1, 0)] were measured to evaluate the response frequency of the whole logic gates. Before each external bias voltage was applied, a 0 V interval was set to make logic gates return to their initial states. As Supplementary Figures 19 and 20 showed, the current under -1.9 V decreased more slowly than that under +1.9 V because of the unidirectional energy storage feature of CAPode. Under -1.9 V, final value of current (1, 1) was always higher than that under +1.9 V. While the logic gates ("AND" and "OR") showed close current responses as the bias voltages were applied under (0, 1) and (1, 0) inputs for different time [Supplementary Figures 21 and 22]. The results demonstrated that the response speed of logic gates based on CAPodes was fast and stable.

As shown in Figure 6H, a LED was switched by an "AND" logic gate based on the CAPodes, where it can be lit up only when both units were under negative bias voltages (1, 1). As for the "OR" logic gate [Figure 6I], the LED can be switched on as the logic gate under states of (1, 1), (1, 0) and (0, 1), and it will be switched off when the both units were applied with positive bias voltage in a state of (0, 0). Furthermore, the outputs of logic gates did not change as the CAPode units were bent to 180° [Supplementary Figure 23], and the I-t curves of logic gates ("AND" and "OR") under different inputs (different bias voltages applied for 5 and 10 s) almost overlapped as the CAPode units were bent to different angles [Supplementary Figure 24], indicating the excellent flexible stability of the logic gates derived from CAPodes. The CAPode–based logic gate

integrated with both functions of current rectification and energy storage does not require other external conducting wires, which can efficiently simplify the structure of logic circuit and reduce the power consumption.

CONCLUSIONS

In conclusion, we have successfully constructed a type of quasi-solid-state CAPodes with high rectification capability and excellent electrochemical performance, and developed flexible logic gates for flexible portable electronics. The unique crystalline structure and charge dual ion sieving effect of MoO_x with abundant negative oxygen vacancies allowed the intercalation of small-size cations (e.g., H^+), providing the MoO_x–based CAPode with both high energy storage ability and rectification capability. By synergistically optimizing the polymer electrolytes, quasi-solid-state flexible CAPode with high performance was developed. With CAPodes used as rectification units and energy supplies, flexible logic gates of "AND" and "OR" with ideal logic operation capability were demonstrated, which represents a promising candidate to be used as integrated units for building complex logic architectures in the field of flexible electric devices in the near future.

DECLARATIONS

Authors' contributions

Conceived the research and supervised the work: Chen, T.
Performed data curation, acquisition, and investigation: Zhai, D.; Yan, Z.; Dong, K.; Tang, W.; Sun, Q.; Li, X.; Yang, J.
Drafted or revised the manuscript: Chen, T.; Zhai, D.; Lv, T.
Provided project administration, and funding acquisition: Chen, T.; Lv T.

Availability of data and materials

All data needed to support the conclusions in the paper are presented in the manuscript and/or the Supplementary Materials. Additional data related to this paper may be requested from the corresponding author upon request.

AI and AI-assisted tools statement

Not applicable.

Financial support and sponsorship

This work was funded by the National Natural Science Foundation of China (No. 22179097, 52272232, and 22575174), and Fundamental Research Funds for the Central Universities (No. 22120220557).

Conflicts of interest

All authors declared that there are no conflicts of interest.

Ethical approval and consent to participate

Not applicable.

Consent for publication

Not applicable.

Supplementary Materials

Supplementary Materials

REFERENCES

1. Shao, H.; Wu, Y. C.; Lin, Z.; Taberna, P. L.; Simon, P. Nanoporous carbon for electrochemical capacitive energy storage. *Chem. Soc. Rev.* **2020**, *49*, 3005-39. DOI
2. Béguin, F.; Presser, V.; Balducci, A.; Frackowiak, E. Carbons and electrolytes for advanced supercapacitors. *Adv. Mater.* **2014**, *26*, 2219-51. DOI PubMed
3. Schütter, C.; Pohlmann, S.; Balducci, A. Industrial requirements of materials for electrical double layer capacitors: impact on current and future applications. *Adv. Energy. Mater.* **2019**, *9*, 1900334. DOI
4. Simon, P.; Gogotsi, Y. Perspectives for electrochemical capacitors and related devices. *Nat. Mater.* **2020**, *19*, 1151-63. DOI PubMed
5. Zhang, P.; Zhu, F.; Wang, F.; et al. Stimulus-responsive micro-supercapacitors with ultrahigh energy density and reversible electrochromic window. *Adv. Mater.* **2017**, *29*, 1604491. DOI PubMed
6. Li, L.; Lou, Z.; Chen, D.; Jiang, K.; Han, W.; Shen, G. Recent advances in flexible/stretchable supercapacitors for wearable electronics. *Small* **2018**, *14*, e1702829. DOI PubMed
7. Dong, K.; Wu, Z.; Deng, J.; et al. A stretchable yarn embedded triboelectric nanogenerator as electronic skin for biomechanical energy harvesting and multifunctional pressure sensing. *Adv. Mater.* **2018**, *30*, e1804944. DOI PubMed
8. Yu, H. C.; Zheng, S. Y.; Fang, L.; et al. Reversibly transforming a highly swollen polyelectrolyte hydrogel to an extremely tough one and its application as a tubular grasper. *Adv. Mater.* **2020**, *32*, e2005171. DOI PubMed
9. Zhang, E.; Fulik, N.; Hao, G. P.; et al. An asymmetric supercapacitor-diode (CAPode) for unidirectional energy storage. *Angew. Chem. Int. Ed. Engl.* **2019**, *58*, 13060-5. DOI PubMed PMC
10. Zhou, H.; Li, P.; Zhang, E.; et al. General design concepts for CAPodes as ionologic devices. *Angew. Chem. Int. Ed. Engl.* **2023**, *62*, e202305397. DOI PubMed
11. Feng, J.; Wang, Y.; Xu, Y.; et al. Construction of supercapacitor-based ionic diodes with adjustable bias directions by using poly(ionic liquid) electrolytes. *Adv. Mater.* **2021**, *33*, e2100887. DOI PubMed
12. Tang, P.; Tan, W.; Li, F.; et al. A pseudocapacitor diode based on ion-selective surface redox effect. *Adv. Mater.* **2023**, *35*, e2209186. DOI PubMed
13. Zhao, G.; Pan, Z.; Xu, Y.; Hou, J.; Kong, L. Unidirectional bias study based on nickel foam electrochemical ion diode. *Adv. Funct. Mater.* **2025**, *35*, 2417394. DOI
14. Bahrawy, A.; Galek, P.; Gellrich, C.; Grothe, J.; Kaskel, S. Advanced redox electrochemical capacitor diode (CAPode) based on parkerite ($Ni_3Bi_2S_2$) with high rectification ratio for iontronic applications. *Adv. Funct. Mater.* **2024**, *34*, 2405640. DOI
15. Feng, J.; Zhang, W.; Batol, A.; et al. Electrochemical capacitance rectification of FeCoCrMnNiP electrode in microcircuit rectification supercapacitor application. *Electrochim. Acta.* **2025**, *533*, 146513. DOI
16. Murugesan, S.; Shreteh, K.; Afik, N.; Alkrenawi, I.; Volokh, M.; Mokari, T. Supercapattery-diode: using layered double hydroxide nanosheets for unidirectional energy storage. *ACS. Appl. Mater. Interfaces.* **2024**, *16*, 49868-79. DOI PubMed
17. Ma, H.; Liang, J.; Qiu, J.; et al. A biocompatible supercapacitor diode with enhanced rectification capability toward ion/electron-coupling logic operations. *Adv. Mater.* **2023**, *35*, e2301218. DOI PubMed
18. Ma, H.; Sun, K.; Cai, Y.; et al. High-rate lithium-ion capacitor diode towards multifrequency ion/electron-coupling logic operations. *Angew. Chem. Int. Ed. Engl.* **2025**, *137*, e202420404. DOI PubMed
19. Bahrawy, A.; Galek, P.; Gellrich, C.; et al. Nanostructured h-WO_3-based ionologic gates with enhanced rectification and transistor functionality. *ACS. Nano.* **2025**, *19*, 20655-71. DOI PubMed PMC
20. Yang, X.; Wu, L.; Ye, L.; et al. Bioinspired high-rate supercapacitor diode for kilohertz computing-in-memory application. *Adv. Funct. Mater.* **2026**, *36*, e24006. DOI
21. Ye, L.; Fu, Y.; Yang, X.; et al. Nanoconfined water manipulated selective proton storage in layered tungsten oxides for versatile supercapacitor diodes. *ACS. Nano.* **2026**, *20*, 6339-51. DOI PubMed
22. Ma, L.; Ma, H.; Sheng, H.; et al. A supercapacitor diode with high rectification ratio induced by carbon and oxygen vacancies. *ACS. Nano.* **2025**, *19*, 19744-56. DOI PubMed
23. Gellrich, C.; Shupletsov, L.; Galek, P.; Bahrawy, A.; Grothe, J.; Kaskel, S. A precursor-derived ultramicroporous carbon for printing iontronic logic gates and super-varactors. *Adv. Mater.* **2024**, *36*, e2401336. DOI PubMed
24. Wang, X.; Huang, S.; Guo, K.; Min, Y.; Xu, Q. Directed and continuous interfacial channels for optimized ion transport in solid-state electrolytes. *Adv. Funct. Mater.* **2022**, *32*, 2206976. DOI
25. Wang, X.; Guo, K.; Xia, Y.; Min, Y.; Xu, Q. Nonstoichiometric molybdenum trioxide adjustable energy barrier enabling ultralong-life all-solid-state lithium batteries. *ACS. Appl. Mater. Interfaces.* **2021**, *13*, 60907-20. DOI PubMed
26. Kim, H. S.; Cook, J. B.; Lin, H.; et al. Oxygen vacancies enhance pseudocapacitive charge storage properties of MoO_{3-x}. *Nat. Mater.* **2017**, *16*, 454-60. DOI PubMed

27. Zhang, X.; Liu, X.; Zeng, Y.; Tong, Y.; Lu, X. Oxygen defects in promoting the electrochemical performance of metal oxides for supercapacitors: recent advances and challenges. *Small. Methods.* **2020**, *4*, 1900823. DOI
28. Zhou, X.; Huang, S.; Gao, L.; et al. Molecular bridging induced anti-salting-out effect enabling high ionic conductive $ZnSO_4$-based hydrogel for quasi-solid-state zinc ion batteries. *Angew. Chem. Int. Ed. Engl.* **2024**, *136*, e202410434. DOI PubMed
29. Tang, C.; Yao, Y.; Li, M.; et al. A new polyvinyl alcohol lithium chloride hydrogel electrolyte: high ionic conductivity and wide working temperature range. *Adv. Funct. Mater.* **2025**, *35*, 2417207. DOI
30. Ma, Y.; Tang, P.; Miao, Z.; et al. Flexible planar micro supercapacitor diode. *J. Energy. Chem.* **2024**, *93*, 429-35. DOI
31. Wei, Y.; Zhao, Y.; Ding, Q.; et al. Hydrogel ionic diode with ultra-high rectification ratio for ionic circuit. *Chem. Eng. J.* **2024**, *498*, 155655. DOI
32. Dong, Q.; Jiang, J.; Wang, Y.; Zhai, J. Geometric tailoring of macroscale $Ti_3C_2T_x$ MXene lamellar membrane for logic gate circuits. *ACS. Nano.* **2021**, *15*, 19266-74. DOI PubMed
33. Wang, Y.; Wang, Z.; Su, Z.; Cai, S. Stretchable and transparent ionic diode and logic gates. *Extreme. Mech. Lett.* **2019**, *28*, 81-6. DOI
34. Feng, X.; Zhao, X.; Yang, L.; et al. All carbon materials pn diode. *Nat. Commun.* **2018**, *9*, 3750. DOI PubMed PMC
35. Zhou, Y.; Hou, Y.; Li, Q.; et al. Biocompatible and flexible hydrogel diode-based mechanical energy harvesting. *Adv. Mater. Technol.* **2017**, *2*, 1700118. DOI
36. Mathwig, K.; Aaronson, B. D. B.; Marken, F. Ionic transport in microhole fluidic diodes based on asymmetric ionomer film deposits. *ChemElectroChem* **2018**, *5*, 897-901. DOI
37. Zhang, W.; Zhang, X.; Lu, C.; Wang, Y.; Deng, Y. Flexible and transparent paper-based ionic diode fabricated from oppositely charged microfibrillated cellulose. *J. Phys. Chem. C.* **2012**, *116*, 9227-34. DOI
38. Wu, J.; Zhan, X.; Hinds, B. J. Ionic rectification by electrostatically actuated tethers on single walled carbon nanotube membranes. *Chem. Commun.* **2012**, *48*, 7979-81. DOI PubMed
39. Cayre, O. J.; Chang, S. T.; Velev, O. D. Polyelectrolyte diode: nonlinear current response of a junction between aqueous ionic gels. *J. Am. Chem. Soc.* **2007**, *129*, 10801-6. DOI PubMed
40. Wan, J.; Lv, T.; Liu, Y.; et al. Flexible asymmetric supercapacitors with extremely slow self-discharge rate enabled by a bilayer heterostructure polymer electrolyte. *Adv. Funct. Mater.* **2022**, *32*, 2108794. DOI
41. Kim, H. J.; Chen, B.; Suo, Z.; Hayward, R. C. Ionoelastomer junctions between polymer networks of fixed anions and cations. *Science* **2020**, *367*, 773-6. DOI PubMed
42. Jiang, F.; Poh, W. C.; Chen, J.; et al. Ion rectification based on gel polymer electrolyte ionic diode. *Nat. Commun.* **2022**, *13*, 6669. DOI PubMed PMC
43. Karnik, R.; Fan, R.; Yue, M.; Li, D.; Yang, P.; Majumdar, A. Electrostatic control of ions and molecules in nanofluidic transistors. *Nano. Lett.* **2005**, *5*, 943-8. DOI PubMed